Highly Monodispersed PbS Quantum Dots for Outstanding Cascaded-Junction Solar Cells

Bo Hou,[†] Yuljae Cho,[†] Byung Sung Kim,[†] John Hong,[†] Jong Bae Park,[‡] Se Jin Ahn,[Δ] Jung Inn Sohn, [†] SeungNam Cha,[†]* Jong Min Kim[§]*

†. Department of Engineering Science, University of Oxford, Parks Road, Oxford OX1 3PJ, UK http://www.eng.ox.ac.uk/nst

‡. Jeonju centre, Korea Basic Science Institute, Jeonju, Jeollabuk-do 54907, Republic of Korea

Δ. New and Renewable Energy Research Division, Photovoltaic Laboratory, Korea Institute of Energy Research (KIER), 152 Gajeong-ro, Yuseong-gu, Daejeon 305-343, Republic of Korea

§. Department of Engineering, University of Cambridge, 9 JJ Thomson Avenue, Cambridge CB3 0FA, UK

ABSTRACT.

High-performance cascaded-junction quantum dot solar cells (CJQDSCs) are fabricated from as-prepared highly monodispersed lead sulphide QDs. The cells have a high power conversion of 9.05% and a short circuit current density of 32.51 $mAcm^{-2}$. A reliable and effective stratagem for fabricating high-quality lead sulphide quantum dots (QD) is explored through a 'monomer' concentration-controlled experiment. Robust QDSC performances with different band gaps are demonstrated from the as-proposed synthesis and processing stratagems. Various potential

CJQDSCs can be envisioned from the band edge evolution of the QDs as a function of size and ligands, reported here.

TOC GRAPHICS

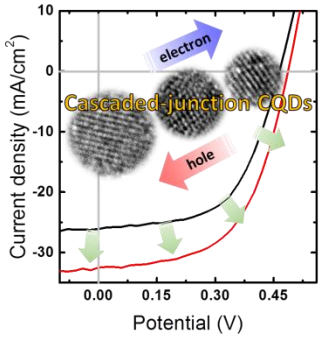

Quantum dots (QDs) are well known as infinitesimal semiconducting nanocrystals with a physical size in the range of their Bohr radius.[1] Due to their discrete density of state, the band gap (ε_{gap}) of QDs can be compatibly modified by manipulating their dimensions, which leads to extensive studies for optoelectronics applications.[2] In particular, facile solution processability and ε_{gap} customisability to the solar spectrum makes QDs one of the most promising materials for future emerging solar cells.[3] Prevalent studies in QD solar cell (QDSC), mainly concern lead sulphide (PbS) materials due to their big Bohr radius (20 nm) and wide band gap (ε_{gap}) tuning range (0.4 eV to 1.5 eV).[4] Profiting from improved process technologies; i.e. better passivation and optimized p-n junction structure, remarkable power conversion efficiencies (PCEs) of ca. 10%, have been achieved recently.[5, 6] However, in spite of the demonstrated abilities and fascinating features in the QDSCs, there are still remaining challenges which need to be

addressed in terms of material quality control and device architecture design.[3] For instance, a vast number of works have been performed to synthesise high-quality PbS QDs,[7, 8] but it is still a challenge to reproduce identical QDs from different batches, which hampers stable device performance. As one of the most promising QD device architectures, solar cells made from cascading various size QD have been proposed and tentatively studied.[9-13] However, due to poor size control of the QDs, so far, none of the works display good PCE performance.

In this work, we elucidate an effective and reliable PbS QD synthesis protocol for fabricating high performance and robust QDSCs. Through adjusting the precursor concentration systematically, in a fixed reaction temperature and quench time, a wide range of different sizes of colloidal PbS QDs is produced with a narrow size distribution and high reproducibility. The effects of quantum-confinement and surface functionalization for different ligands and QD size is subject to a rationalisation analysis. Finally, based on the understanding gained of the optical-electrical properties of as-prepared PbS QDs, three distinct sizes of PbS QDs are selected and fabricated into cascaded-junction solar cells (CJSC) under ambient air conditions. The device structure is illustrated in Figure 1a, which employs layers of different size QDs treated with different ligands for tuning their relative band alignment and also photon energies absorption. The elaborately designed devices show impressive high PCE and short circuit current density compared with previously reported devices. [5, 6]

The assembling of CJSC requires highly monodispersed PbS QDs with a range of different possible sizes, ensuring small coplanar charge transport barriers and distinct size-dependent optical properties.[2] QDs utilised in the light absorber layers shall be selected from the best performance single ε_{gap} QDSC, which possess high values of PCE and quantum efficiency. Through the size and ligand engineering, the band alignments of the selected QDs shall also

facilitate effective dissociation of excitons and transfer of the photo-generated charge carriers towards the corresponding cathode and anode in the QDSCs. To these ends, we firstly look into investigating a reproducible preparation approach for highly monodispersed PbS QDs together with optimising single ε_{gap} QDSCs, since they are critical steps towards our proposed theme.

PbS QDs were prepared based on a conventional 'hot-injection' approach employing a Schlenk line technique,[7] but our monomer concentration control (MCC) method resulted in monodispersed PbS QDs with high reproducibility which is crucial for QD and device manufacturing. Unlike previous works, [7, 14] the loading of mole ratio between lead oxide (PbO) and (oleic acid) OA were deliberately set as PbO to OA equal to 1:2, 1:3, 1:5, 1:8, 1:11, 1:14, 1:17 and 1:27, respectively. During the synthesis, other parameters which are strongly related to control the size of the QDs were fixed with 20 seconds reaction time and 130 ºC injection temperature. The reaction time is controlled by quenching the reaction with an ice bath rather than allowing it to cool down naturally. This reliable and modularized synthesis process of PbS QDs over a wide range of targeted size is attributed to good control of the 'critical size'.[15] By changing the PbO:OA mole ratio to manipulate the PbS monomer concentration, the size of as-prepared PbS QDs can be precisely controlled. A high PbS monomer concentration in the nucleation stage induced a small size of PbS QDs and a low PbS monomer concentration induced a big size of PbS QDs. Our experimental results on the size controllability can be supported by the colloid growth theory:[15] i) The nanocrystal growth time is fixed to 20 seconds which means the overall QDs growth time is transient i.e. the 'Nucleation stage' is dominating rather than the 'Riping stage'.[16] ii) The OA amount is adjusted during the PbS QDs synthesis, which implies that the amount of lead monomer and the sulfur monomer remain fixed but the monomer concentration is changed depending on the OA's loading. Just as in Sugimoto model of

the growth rate versus size plot,[17] the high initial monomer concentration induces a bigger 'critical size' and leads to a slow growth rate of the particle (all the particles smaller than the 'critical size' have a negative growth rate). Eventually, the high initial monomer concentration results in the formation of small-sized QDs for the fixed reaction time. In a low initial monomer concentration (as the increment of OA amount), the smaller 'critical size' induces the very fast growth rate of the particles (particles formed at the nucleation stage which are bigger than the 'critical size' have a positive growth rate). Ultimately, low initial monomer concentrations induce the formation of large PbS QDs for the fixed reaction time.

Absorption spectroscopy analysis was carried out to evaluate the size distribution and ε_{gap} variation of the as-prepared PbS QDs. As shown in Figure 1b, the ε_{gap} obtained from as-prepared QDs can cover from 0.84 eV to 1.37 eV which encompasses the optimal energy gap for a single junction cell (Shockley-Queisser limit, ca. 1.3 eV).[18] A group of transmission electron microscopy (TEM) images (20 nm scale bar) of four different sizes of PbS QDs with the corresponding ε_{gap} from 0.84 eV to 1.37 eV are exhibited in inset image of Figure 1b. It can be seen that the as-prepared PbS QDs show a clear monodispersity among different ε_{gap}. The monodispersity of PbS QDs is evaluated from a full width at half maximum (FWHM) of the absorption spectrum and the standard deviation (Std. Dev.) of the TEM size distribution. Regardless of the QD size, a sharp narrow first exciton peak is a common feature in Figure 1b, and the FWHM of the peaks ranges from 100 to 150 nm (Figure 1c). Based on the particle size TEM statistical calculations, the as-prepared PbS QDs possess a Std. Dev. below 0.65 nm (detail TEM analysis can be found in the supporting information SIV Figure S1 to Figure S7). Comparing with FWHM values from previous reports (e.g. 100 ~ 275 nm), as can be seen in the Figure 1c, our MCC method produced highly monodispersed QDs with identical or smaller

FWHM values.[14, 19-22] It should be noted that the variation of Std. Dev. (blue circles) and FWHM (black circles) as a function of QD size is also very small (as shown in Figure 1c). These experimental results on the monodispersity of QDs fit well with the theoretical simulations in Talapin's report which show that by adjusting the initial monomer concentration, a minimization of Std. Dev. as a function of size is expected.[16] That is, an adjustment of monomer concentration accompanied with a change in targeted QD size can bridge the gap of the 'focusing', 'defocusing' or 'equilibrium' processes during the growth of colloidal particle, which ultimately contributes to the uniform size monodispersity.[16] Two representative PbS QDs with ε_{gap} 1.37 eV and 0.84 eV (0.84 eV QD shown in the supporting information SV, Figure S9) were fabricated through conventional time-dependent method (CM) and MCC experiments. It can be seen from Figure 1d that the first exciton peak from the absorption spectrum shows a narrowing trend (as indicated by the arrows) between the MCC and CM. The peak to valley ratio is also enlarged when employing the MCC method. The peak to valley ratios among the different size of QDs extracted from the absorption spectra is within 3.5 to 2 as shown in the supporting information SV (Figure S9b).

The high crystallinity and the rock-salt cubic crystal structure of as-prepared PbS QDs are demonstrated from high-resolution TEM (HRTEM), selected area diffraction (SAED) and x-ray diffraction (XRD) analysis. The SAED pattern and HRTEM images in Figure 1e-f were taken from 0.84 eV PbS QDs, the other ε_{gap} PbS QDs microscopy studies and XRD analysis can be found in the support Information SIV (Figure S1-S8a). In Figure 1e, typical polycrystalline continuous ring SAED patterns are clearly resolved. As indexed in the diffraction pattern, the main lattice diffractions are arising from {111}, {200}, {220}, {222}, {420} and {511} planes. An average value of the lattice constant, *a,* computed from each reflection is 5.89±0.05 Å, which

is quite close to the reported PbS bulk values 5.936 Å.[23] Regarding individual particles, the HRTEM study was performed to understand the microstructure of the as-prepared QDs. As shown in Figure 1f, (111) and (200) and (220) planes can be readily indexed, and the lattice distances of these planes are measured to be 3.42±0.01 Å, 2.9±0.01 Å, and 2.1±0.01 Å respectively, which gives a lattice constant of cubic PbS *a*=5.89±0.02 Å. A cross-grating pattern was also resolved as highlighted in Figure 1f, the angle between (111) and (200) planes are measured to be 55 ±1 ° which further demonstrated the PbS QD cubic feature. Guidance for the preparation of each size of PbS QD as a function of OA: PbO mole ratio is also provided in the supporting information (Figure S8b). As can be seen from the Figure S8b, the diameter of as-prepared PbS QDs, measured from TEM, XRD (calculated from Scherrer equation) and computed from the empirical equation,[24] are found to correlate well with each other.

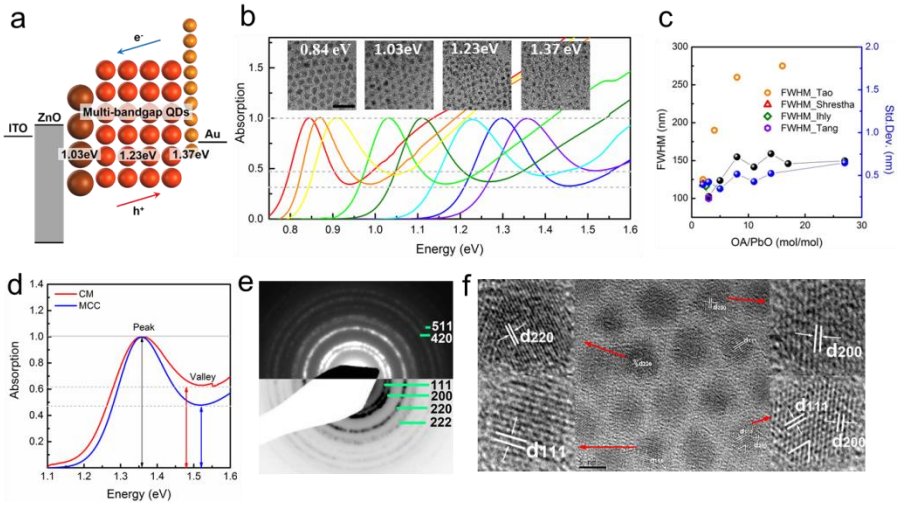

Figure 1 a) Schematic of the proposed cascaded-junction cell with optimum combination of PbS QDs. b) Optical absorption spectra of different size of PbS QDs synthesis from a series of control experiments. The values of optical ε_{gap} of PbS QDs range from 1.37 eV to 0.84 eV, and the corresponding mole ratio between OA to PbO ranges from 2:1 to 27:1. Inset TEM images of as-prepared PbS QDs with different optical ε_{gap}, the scale bar in the images are equal to 20nm. Horizontal short dashed lines are the reference lines for calculating peak to valley ratios. c) FWHM (black) and TEM size variation results (blue) obtained from the optical absorption spectra and TEM size distribution analysis. Colour symbols are previous reported values.[19-22] d) Comparison of the first exciton peak of 1.37 eV PbS QDs synthesised from CM method (red curve) and MCC method (blue curve), curve arrows indicate the narrowing trend between the two approaches. Vertical arrows indicate the peak to valley ratio between CM (1.61) and MCC (2.2) methods. e-f) SAED and HRTEM images of as-prepared 0.84 eV PbS QDs, scale bar equals to 5 nm.

In our optimized cell fabrication condition, ZnO film, a hole block layer in QDSC, is fabricated by spin-coated ZnO nanoparticles (NPs) with an additional thermal annealing procedure. We

attribute the benefits of the annealing to the increment of band offset (140 meV) between ZnO and adjacent QD layers, which provides an energy barrier that prevents photo-generated electrons flowing back to the QD layer. Ultraviolet photoelectron spectroscopy (UPS) analysis (Figure 2a) reveals the effects of annealing on the position of the ZnO film band edges and detailed discussions can be found in the Figure S10 and supporting information SVI. Figure 2b exhibits four representative J-V curves of as-fabricated single junction PbS QDSCs. Accompanied by changing ε_{gap} from 0.84 eV to 1.37 eV, perceptible increments of open circuit voltage (V_{oc}) can be resolved from the intersections of the abscissa with the x-axis.[25] Figure 2c displays PCE values of the single junction QDSCs fabricated from different sizes of QDs, and the highest PCE values fabricated under our optimized condition is found from 1.23 eV PbS QDs. Essential parameters such as V_{oc}, J_{sc}, series resistance (R_s), shunt resistance (R_{sh}), fill factor (FF) and PCE values are extracted from the J-V curves and listed in Table 1 (The J_{SC} values calculated by integrating the EQE spectra with the AM 1.5 G TILT (ASTM-G173-03) solar spectrum are also listed in the supporting information SVII, Table S1). From Table 1 it can be derived that R_{sh} shows a size-dependent trend which may be closely related to the size-dependent quantum confinement of the QDs. Larger PbS QDs (smaller ε_{gap}) show bigger R_{sh} values (i.e. low leakage current), which suggests weak quantum confinement which would induce lower leakage current or charge carrier pathways in QDs and vice versa.[26] Therefore, it indicates introducing larger QDs into QDSCs may help improve R_{sh}, subsequently decrease leakage current. Figure 2d shows the peak external quantum efficiency (EQE) as a function of ε_{gap} (full EQE spectra can be found in the supporting information SVII, Figure S11, and Figure S12).

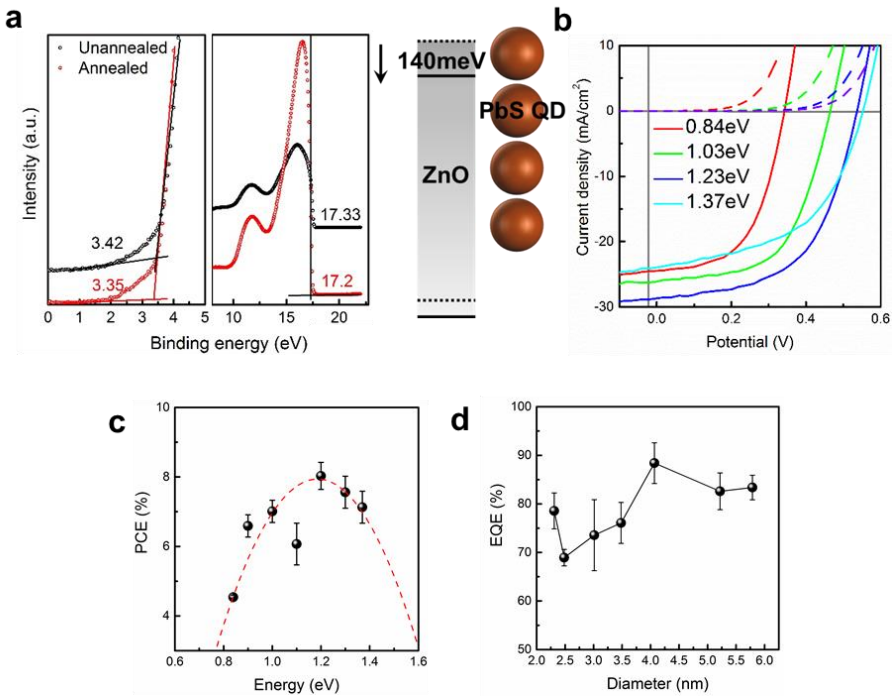

Figure 2 a) UPS spectra of unannealed ZnO film (black curve) and annealed ZnO (red curve) film. The left panel shows magnified spectra near Fermi edge and right panel shows the secondary electron cut-off region. Spectra were shifted for clarity and the identified binding energy values are listed besides each plot. ε_{gap} of annealed (bulk) and as-prepared ZnO NPs are employed as 3.37 eV and 3.45 eV respectively.[27] The band alignment schematic of annealed (solid line) and unannealed (dotted line) ZnO NPs film relative to 1.3 eV PbS@TBAI at open-circuit conditions is also provided to exemplify the band edge shift. b) Representative J-V curves of QDSC with PbS QDs ε_{gap} of 0.84 eV (red curves), 1.03 eV (green curves), 1.23 eV (blue curves) and 1.37 eV (light blue) under Dark (dashed line) and 1.5 AM illumination (continuous line). c) PCE values (black legend) evolution as a function of QDs optical ε_{gap}, the red dotted line is a Gaussian data fitting for guiding the PCE changing trend, error bar generated from standard deviation of parallel optimized solar cells. d) Peak EQE values measured at 400 nm wavelength as a function of ε_{gap}, error bar generated from multiple parallel solar cells measurement.

Size-dependent band edge (ε_{edge}) variation of PbS QDs stabilised with two prevailing ligands (i.e. tetrabutylammonium iodide, PbS@TBAI and 1, 2-ethanedithiol, PbS@EDT) are also studied by the UPS measurement. As shown in Figure 3, the conduction band edge (ε_C) and valence band edge (ε_V) evolve as a function of PbS QDs size, exhibiting different behaviour between the TBAI (Figure 3a) and EDT (Figure 3b) functionalization. In the case of TBAI capped PbS QDs, the ε_C energy level dropped at a similar rate with the increasing of ε_V energy levels resulting in a convergence of energy levels as a function of QD size. This type of ε_{edge} variation (i.e. convergence) is consistent with the identical small effective mass of electron and hole in lead salts, which induces large confinement energies split about equally between carriers.[4] On the other hand, the EDT capped PbS QDs display a different trend to TBAI capped ones. In Figure

3b, the ε_V energy levels of the EDT treated PbS QDs only subtly change (remaining nearly steady) as the size of QDs varied, but the ε_C energy levels change dramatically.[28] The different behaviours of ε_{edge} energy levels variation between TBAI and EDT treated PbS QDs can be attributed to the stoichiometry transformation. The atomic ratios of Pb and S analysed by quantized X-ray photoelectron spectroscopy (XPS) from different ligands show that the TBAI decoration only brought negligible changing of Pb/S ratio but the treatment of EDT dramatically modified the Pb/S ratio from Pb-rich to S-rich (Figure 3c and Supporting information SXIII, Figure S13, and Table S2).[29] On the basis of the previous reported first principle calculations, the inception of this is related to the animalus nature of the the lead chalcogenide relative to the conventional zinc-blende II-VI and III-V compounds.[30, 31] For instance, the Pb *6s* band was found to lie below the top of the valence band and the existence of an occupied Pb *s* band leads the S *p* orbitals also to contribute to the conduction band.[30, 31] Consequently, a strong S *p* and Pb *s* coupling (L point in the Brillouin zone) facilitate a 'balancing act' that induce a conduction band more sensitive to the anion variation.[30, 31] This finding suggests a modification of stoichiometry of PbS QDs (from surface or integrity) shall have a remarkable effect on the electronic structure of PbS QDs.[32] Furthermore, the ε_{edge} diagrams of TBAI or EDT functionalised QDs, are actually an guidance for CJQDSC fabrication, since type II junctions can be easily formed between PbS@TBAI and PbS@EDT QDs, or even PbS@EDT QDs themselves. These CJQDSCs combine 'junction', 'ligand' and 'QD size' effects into one case, which can promote wider photon energies absorption and higher electron-hole pair splitting efficiency. Specifically, in this type of QDSC, photons of different energies can be absorbed preferentially in layers of different ε_{gap}, so the loss of electronic kinetic energy and extracted electrochemical potential can also be effectively reduced.[25] Moreover, employing QDs with

different ε_{gap} but made of the same substance can result in the minimisation of the lattice mismatch and enhancement of the built-in electric field between junctions.[25]

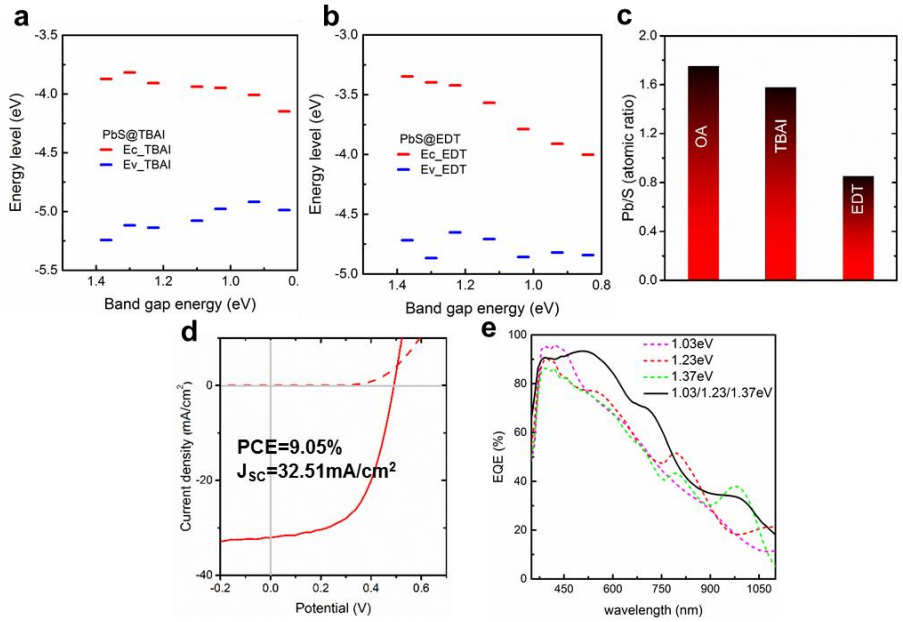

Figure 3 Size dependence of the ε_{edge} energy (ε) vs vacuum of PbS QDs capped by TBAI (PbS@TBAI) a) and EDT (PbS@EDT) b). c) Quantized XPS results of the atomic ratio between Pb and S after decorating PbS with different ligands. d) J-V curves of a champion CJQDSC with PbS QDs ε_{gap} of 1.03 eV/1.23 eV/1.37 eV under Dark (dashed line) and 1.5 AM illumination (continuous line). Inset text highlighted the champion cell PCE performance. e) Represented EQE spectra of single ε_{gap} QDSC (dashed line) and multiple ε_{gap} CJQDSC (solid line). Specification for each solar cell ε_{gap} values is indicated in the image.

Based on aforementioned systematic studies on the properties of QDs and QDSCs, three distinct sizes of QDs (PCE champion 1.23 eV QDs, the Shockley-Queisser limit preferred 1.37 eV QD and high EQE 1.03 eV QD) were selected for the fabrication of CJQDSCs. In consideration of size difference of the QDs, QD film thicknesses are evaluated by atomic force microscopy and scanning electron microscope (supporting information SIX, Figure S14, and Figure S15) before each type of solar cell fabrication. Typically, in the CJQDSC, a layer of the 1.03 eV QD@TBAI serves as absorber and hole-extractor, 10 layers of 1.23 eV QD acts as the main light absorbing layer and a layer of 1.37 eV QD serves as an electron-blocking/hole-extracting layer (detailed solar cell fabrication procedures can be found in the experimental section). As shown in Figure

3d, we successfully demonstrate that the CJQDSC can generate a 9.05% PCE performance, which is higher than any of its constituent QDSCs, with a particularly outstanding high J_{sc} and high R_{sh}. Figure 3e shows EQE performances of the typical CJQDSC and its component individual solar cells. The highest EQE comes from the 1.03 eV QDSC, but the CJQDSC shows the best spectrum coverage and higher EQE performance than the 1.23 eV and 1.37 eV QDSCs. As a result of the improved optical absorption (Supporting information, Figure S16), the J_{sc} values of CJQDSCs can be increased up to 32.51 $mAcm^{-2}$ which is the highest value among any reported values in PbS QDSCs.[5, 6] The J_{SC} value calculated by integrating the EQE spectra with the AM1.5G solar spectrum for CJQDSC is 30.11 mA/cm^2 (28.01±2.10 mA/cm^2) which shows a good agreement with the measured J_{SC}. Furthermore, the PbS CJQDSC shows a robust stability, it can be fabricated in the air condition but retains a high PCE performance under ambient air condition for more than 20 weeks (Supporting information SX, Figure S17).

Comparisons between our single ε_{gap} cells, CJQDSCs, and world leading results are listed in Table 1. In spite of the promising performance of our CJQDSCs, there are still a vast number of parameters which can be optimized to catch up the world leading devices. For example, our FF and V_{oc} values are smaller than the world best cell, which may result from a poor packing density and interface defects. On-going works such as improving QD layers packing densities, reducing multiple junction interface potential barriers, and tackling the V_{oc} deficiency[32] are carried out in our group.

Table 1. Summarization of V_{oc}, J_{sc}, R_s, R_{sh}, FF and PCE average values of as-prepared solar cells correlated with QDs optical ε_{gap}, champion devices are quoted in the brackets. Single junction QDSC results are averaged across 9 samples on 3 different substrates. CJQDSC results are averaged across 30 samples on 10 different substrates. PCE of champion devices are quoted in brackets. [a] values are cited from reference 6 (Chuang et al.) which is the first reported high-performance PbS QDSC above 8% PCE. [b] values are cited from reference 5 (Lan et al.) which is the world record PbS QDSC with 10.18% PCE.

Type	ε_{gap}(eV)	V_{oc}(V)	J_{sc}($mAcm^{-2}$)	R_s(Ωcm^2)	R_{sh}(Ωcm^2)	FF	PCE (%)

QDSC	0.84	0.35±0.01 (0.36)	22.66± 1.39(24.47)	4.54±2.79 (4.88)	314.07±32.99 (311.79)	0.57±0.02 (0.59)	4.54±0.06 (4.60)
QDSC	0.91	0.44±0.01 (0.46)	27.58±1.34 (29.63)	8.47±2.86 (7.04)	296.19±23.99 (317.06)	0.54±0.01 (0.55)	6.59±0.32 (7.06)
QDSC	1.03	0.47±0.01 (0.48)	25.46±1.05 (26.75)	3.49±1.84 (6.82)	267.64±20.00 (239.04)	0.59±0.02 (0.6)	7.01±0.32 (7.28)
QDSC	1.14	0.53±0.01 (0.54)	22.70±1.92 (25.36)	8.34±1.94 (8.59)	213.28±24.86 (255.30)	0.50±0.02 (0.53)	6.07±0.60 (6.89)
QDSC	1.23	0.54 (0.54)	26.77±1.77 (28.86)	5.39±1.55 (5.26)	253.46±30.08 (264.76)	0.56±0.02 (0.58)	8.03±0.39 (8.55)
QDSC	1.30	0.58±0.02 (0.60)	24.48±1.15 (26.39)	5.80±1.73 (4.32)	197.99±19.41 (198.59)	0.54±0.03 (0.57)	7.56±0.46 (8.07)
QDSC	1.37	0.55±0.01 (0.56)	26.06±1.34 (27.52)	9.17±2.22 (7.85)	181.40±33.87 (226.78)	0.49±0.02 (0.51)	7.13±0.46 (7.63)
CJQDSC	1.03/1.23/1.37	0.50±0.02 (0.52)	31.24±0.92 (32.51)	4.60±1.70 (4.30)	304.35±14.52 (318.249)	0.56±0.03 (0.59)	8.67±0.28 (9.05)
QDSC[a]	1.33	0.55	26.5	-	-	0.63	8.55
QDSC[b]	1.37	0.64	22.6	-	-	0.73	10.18

In summary, highly monodispersed PbS QDs are fabricated from the MCC method. Experimentally, the size deviation of the as-prepared QD is demonstrated to be smaller than the CM approach. Annealed zinc oxide layer is found to be of benefit for ensuring the robust performance of QDSCs and 1.23 eV PbS QD shows the best single-junction solar cell performance in our optimized conditions. From UPS analysis, distinct ε_{edge} shifting trends are discovered between TBAI and EDT treated PbS QDs, which are attributed to the stoichiometry variation during the ligand exchange. In view of the appropriate band alignments among various ε_{gap} QDs, the CJQDSC prototype is proposed and successfully constructed. In the end, we demonstrate the credibility of these multiple ε_{gap} homojunction solar cells by its outstanding photovoltaic performance. We believe the MCC QD synthesis protocol and CJQDSC model can be a promising candidate encouraging future high-performance QDSC studies.

ASSOCIATED CONTENT

Supporting Information. Experimental sections include the preparation methods of materials and devices. Material and device characterizations such as microscopes, diffractions, ultraviolet photoelectron spectroscopy, x-ray photoelectron spectroscopy and external quantum efficiencies can also be found in the supporting information.

AUTHOR INFORMATION

Corresponding Authors

*junginn.sohn@eng.ox.ac.uk, *seungnam.cha@eng.ox.ac.uk

Notes

The authors declare no competing financial interest.

ACKNOWLEDGMENT

The research leading to these results has received funding from the European Research Council under ERC Grant Agreement n. 340538. The authors would also like to thank the financial support from the National Research Foundation (NRF) of Korea (2015M2A2A6A02045252) and the framework of Research and Development Program of the Korea Institute of Energy Research (KIER, B6-2498).

REFERENCES

(1) Brus, L. E. Electron–Electron and Electron-Hole Interactions in Small Semiconductor Crystallites: the Size Dependence of the Lowest Excited Electronic State. *J. Chem. Phys.* **1984,** *80*, 4403-4409.
(2) Konstantatos G; Sargent E. H. *Colloidal Quantum Dot Optoelectronics and Photovoltaics*. Cambridge University Press: 2013.
(3) Kim, M. R.; Ma, D. Quantum-Dot-Based Solar Cells: Recent Advances, Strategies, and Challenges. *J. Phys. Chem. Lett.* **2015,** *6*, 85-99.

(4) Wise, F. W. Lead Salt Quantum Dots: the Limit of Strong Quantum Confinement. *Acc. Chem. Res.* **2000,** *33*, 773-780.
(5) Lan, X.; Voznyy, O.; Kiani, A.; García de Arquer, F. P.; Abbas, A. S.; Kim, G.-H.; Liu, M.; Yang, Z.; Walters, G.; Xu, J., et al. Passivation Using Molecular Halides Increases Quantum Dot Solar Cell Performance. *Adv. Mater.* **2015**, 28, 299–304.
(6) Chuang, C.-H. M.; Brown, P. R.; Bulović, V.; Bawendi, M. G. Improved Performance and Stability in Quantum Dot Solar Cells through Band Alignment Engineering. *Nat. Mater.* **2014,** *13*, 796-801.
(7) Hines, M. A.; Scholes, G. D. Colloidal PbS Nanocrystals with Size-Tunable Near-Infrared Emission: Observation of Post-Synthesis Self-Narrowing of the Particle Size Distribution. *Adv. Mater.* **2003,** *15*, 1844-1849.
(8) Cademartiri, L.; Bertolotti, J.; Sapienza, R.; Wiersma, D. S.; von Freymann, G.; Ozin, G. A. Multigram Scale, Solventless, and Diffusion-Controlled Route to Highly Monodisperse PbS Nanocrystals. *J. Phys. Chem. B* **2006,** *110*, 671-673.
(9) Neo, D. C. J.; Stranks, S. D.; Eperon, G. E.; Snaith, H. J.; Assender, H. E.; Watt, A. A. R. Quantum Funneling in Blended Multi-Band Gap Core/Shell Colloidal Quantum Dot Solar Cells. *Appl. Phys. Lett.* **2015,** *107*, 103902.
(10) Choi, J. J.; Wenger, W. N.; Hoffman, R. S.; Lim, Y.-F.; Luria, J.; Jasieniak, J.; Marohn, J. A.; Hanrath, T. Solution-Processed Nanocrystal Quantum Dot Tandem Solar Cells. *Adv. Mater.* **2011,** *23*, 3144-3148.
(11) Santra, P. K.; Kamat, P. V. Tandem-Layered Quantum Dot Solar Cells: Tuning the Photovoltaic Response with Luminescent Ternary Cadmium Chalcogenides. *J. Am. Chem. Soc.* **2013,** *135*, 877-885.
(12) Semonin, O. E.; Luther, J. M.; Beard, M. C. Quantum Dots for Next-Generation Photovoltaics. *Mater. Today* **2012,** *15*, 508-515.
(13) Wang, X.; Koleilat, G. I.; Tang, J.; Liu, H.; Kramer, I. J.; Debnath, R.; Brzozowski, L.; Barkhouse, D. A. R.; Levina, L.; Hoogland, S., et al. Tandem Colloidal Quantum Dot Solar Cells Employing a Graded Recombination Layer. *Nat Photon* **2011,** *5*, 480-484.
(14) Zhang, J.; Crisp, R. W.; Gao, J.; Kroupa, D. M.; Beard, M. C.; Luther, J. M. Synthetic Conditions for High-Accuracy Size Control of PbS Quantum Dots. *J. Phys. Chem. Lett.* **2015,** *6*, 1830-1833.
(15) Peng, X.; Wickham, J.; Alivisatos, A. P. Kinetics of II-VI and III-V Colloidal Semiconductor Nanocrystal Growth: "Focusing" of Size Distributions. *J. Am. Chem. Soc.* **1998,** *120*, 5343-5344.
(16) Talapin, D. V.; Rogach, A. L.; Haase, M.; Weller, H. Evolution of an Ensemble of Nanoparticles in a Colloidal Solution: Theoretical Study. *J. Phys. Chem. B* **2001,** *105*, 12278-12285.
(17) Sugimoto, T. Preparation of Monodispersed Colloidal Particles. *Adv. Colloid Interface Sci.* **1987,** *28*, 65-108.
(18) Shockley, W.; Queisser, H. J. Detailed Balance Limit of Efficiency of p-n Junction Solar Cells. *J. Appl. Phys.* **1961,** *32*, 510-519.
(19) Ihly, R.; Tolentino, J.; Liu, Y.; Gibbs, M.; Law, M. The Photothermal Stability of PbS Quantum Dot Solids. *ACS Nano* **2011,** *5*, 8175-8186.
(20) Shrestha, A.; Jin, B.; Kee, T. W.; Qiao, S. Z.; Dai, S. A Robust Strategy for "Living" Growth of Lead Sulfide Quantum Dots. *ChemNanoMat* **2015**, *2*, 49–53.

(21) Tao, L.; Xiong, Y.; Liu, H.; Shen, W. High Performance PbS Quantum Dot Sensitized Solar Cells via Electric Field Assisted in situ Chemical Deposition on Modulated TiO_2 Nanotube Arrays. *Nanoscale* **2014,** *6*, 931-938.
(22) Tang, J.; Brzozowski, L.; Barkhouse, D. A. R.; Wang, X.; Debnath, R.; Wolowiec, R.; Palmiano, E.; Levina, L.; Pattantyus-Abraham, A. G.; Jamakosmanovic, D., et al. Quantum Dot Photovoltaics in the Extreme Quantum Confinement Regime: The Surface-Chemical Origins of Exceptional Air- and Light-Stability. *ACS Nano* **2010,** *4*, 869-878.
(23) Madelung, O.; Rössler, U.; Schulz, M., *Non-Tetrahedrally Bonded Elements and Binary Compounds I: Lead sulfide (PbS) crystal structure, lattice parameters, thermal expansion*. Springer Berlin Heidelberg: 1998.
(24) Moreels, I.; Lambert, K.; Smeets, D.; De Muynck, D.; Nollet, T.; Martins, J. C.; Vanhaecke, F.; Vantomme, A.; Delerue, C.; Allan, G., et al. Size-Dependent Optical Properties of Colloidal PbS Quantum Dots. *ACS Nano* **2009,** *3*, 3023-3030.
(25) Nelson, J., *The Physics of Solar Cells*. Imperial College Press: 2003.
(26) Yoon, W.; Boercker, J. E.; Lumb, M. P.; Placencia, D.; Foos, E. E.; Tischler, J. G. Enhanced Open-Circuit Voltage of PbS Nanocrystal Quantum Dot Solar Cells. *Sci. Rep.* **2013,** *3*, 2225.
(27) Masuda, Y.; Yamagishi, M.; Seo, W. S.; Koumoto, K. Photoluminescence from ZnO Nanoparticles Embedded in an Amorphous Matrix. *Crystal Growth & Design* **2008,** *8*, 1503-1508.
(28) Jasieniak, J.; Califano, M.; Watkins, S. E. Size-Dependent Valence and Conduction Band-Edge Energies of Semiconductor Nanocrystals. *ACS Nano* **2011,** *5*, 5888-5902.
(29) Kim, D.; Kim, D.-H.; Lee, J.-H.; Grossman, J. C. Impact of Stoichiometry on the Electronic Structure of PbS Quantum Dots. *Phys. Rev. Lett.* **2013,** *110*, 196802.
(30) Hou, B.; Parker, D.; Kissling, G. P.; Jones, J. A.; Cherns, D.; Fermín, D. J. Structure and Band Edge Energy of Highly Luminescent $CdSe_{1-x}Te_x$ Alloyed Quantum Dots. *J. Phys. Chem. C* **2013,** *117*, 6814-6820.
(31) Wei, S.-H.; Zunger, A. Electronic and structural anomalies in lead chalcogenides. *Physical Review B* **1997,** *55*, 13605-13610.
(32) Chuang, C.-H. M.; Maurano, A.; Brandt, R. E.; Hwang, G. W.; Jean, J.; Buonassisi, T.; Bulović, V.; Bawendi, M. G. Open-Circuit Voltage Deficit, Radiative Sub-Bandgap States, and Prospects in Quantum Dot Solar Cells. *Nano Lett.* **2015,** *15*, 3286-3294.